Cell

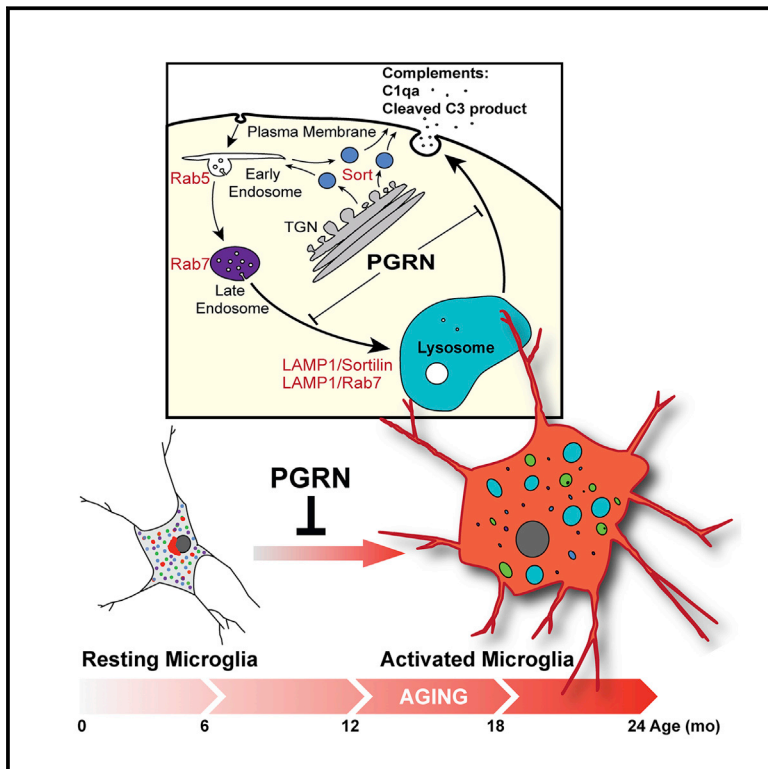# Progranulin Deficiency Promotes Circuit-Specific Synaptic Pruning by Microglia via Complement Activation

Graphical Abstract

Highlights

- Progranulin regulates lysosomal function and complements production in microglia

- $Grn^{-/-}$ microglia preferentially eliminates inhibitory synapse in ventral thalamus

- $Grn^{-/-}$ mice exhibit hyperexcitability in ventral thalamus and OCD-like behaviors

- Loss of C1qa mitigates neurodegeneration and improves survival in $Grn^{-/-}$ mice

Authors

Hansen Lui, Jiasheng Zhang, Stefanie R. Makinson, ..., Jeanne T. Paz, Ben A. Barres, Eric J. Huang

Correspondence

eric.huang2@ucsf.edu

In Brief

Loss of progranulin, which occurs in patients with frontotemporal dementia, causes lysosomal defects and excessive complement production, triggering selective synaptic pruning by microglia and behavioral deficits that can be rescued by blocking complement activation.

Accession Numbers

GSE75083

CrossMark

CellPress

Progranulin Deficiency Promotes Circuit-Specific Synaptic Pruning by Microglia via Complement Activation

Hansen Lui,[1,18] Jiasheng Zhang,[1] Stefanie R. Makinson,[2] Michelle K. Cahill,[1] Kevin W. Kelley,[3] Hsin-Yi Huang,[1,19] Yulei Shang,[1] Michael C. Oldham,[4] Lauren Herl Martens,[5] Fuying Gao,[6] Giovanni Coppola,[6] Steven A. Sloan,[7] Christine L. Hsieh,[8] Charles C. Kim,[9,20] Eileen H. Bigio,[10] Sandra Weintraub,[10] Marek-Marsel Mesulam,[10] Rosa Rademakers,[11] Ian R. Mackenzie,[12] William W. Seeley,[13] Anna Karydas,[13] Bruce L. Miller,[13] Barbara Borroni,[14] Roberta Ghidoni,[15] Robert V. Farese, Jr.,[16] Jeanne T. Paz,[2] Ben A. Barres,[7] and Eric J. Huang[1,17,*]

[1]Department of Pathology, University of California, San Francisco, San Francisco, CA 94143, USA
[2]Gladstone Institute of Neurological Disease and Department of Neurology, University of California, San Francisco, San Francisco, CA 94158, USA
[3]Medical Scientist Training Program, University of California, San Francisco, San Francisco, CA 94143, USA
[4]Department of Neurological Surgery, University of California, San Francisco, San Francisco, CA 94158, USA
[5]FORUM Pharmaceuticals, Waltham, MA 02451, USA
[6]Semel Institute for Neuroscience and Human Behaviors, University of California, Los Angeles, Los Angeles, CA 90095, USA
[7]Department of Neurobiology, Stanford University School of Medicine, Stanford, CA 94305, USA
[8]Immunology Section, San Francisco VA Medical Center and Department of Medicine, University of California, San Francisco, San Francisco, CA 94121, USA
[9]Department of Medicine, University of California, San Francisco, San Francisco, CA 94110, USA
[10]Northwestern Alzheimer Disease Center, Northwestern University Feinberg School of Medicine, Chicago, IL 60611, USA
[11]Department of Neuroscience, Mayo Clinic, Jacksonville, FL 32224, USA
[12]Department of Pathology, University of British Columbia and Vancouver General Hospital, Vancouver, BC V5Z 1M9, Canada
[13]Department of Neurology and Memory and Aging Center, University of California, San Francisco, San Francisco, CA 94158, USA
[14]Centre for Ageing Brain and Neurodegenerative Disorders, Neurology Unit, University of Brescia, Brescia 25100, Italy
[15]Molecular Markers Laboratory, IRCCS Istituto Centro San Giovanni di Dio, Fatebenefratelli, Brescia 25100, Italy
[16]Department of Genetics and Complex Diseases, School of Public Health, Harvard University, Boston, MA 02115, USA
[17]Pathology Service (113B), San Francisco VA Medical Center, San Francisco, CA 94121, USA
[18]Present address: UC Berkeley-UCSF Joint Medical Program (JMP), School of Public Health, Berkeley, CA 94720, USA
[19]Present address: Department of Pathology, National Taiwan University Hospital, Taipei 10002, Taiwan
[20]Present address: Verily, Mountain View, CA 94043, USA
*Correspondence: eric.huang2@ucsf.edu
http://dx.doi.org/10.1016/j.cell.2016.04.001

SUMMARY

Microglia maintain homeostasis in the brain, but whether aberrant microglial activation can cause neurodegeneration remains controversial. Here, we use transcriptome profiling to demonstrate that deficiency in frontotemporal dementia (FTD) gene progranulin (Grn) leads to an age-dependent, progressive upregulation of lysosomal and innate immunity genes, increased complement production, and enhanced synaptic pruning in microglia. During aging, $Grn^{-/-}$ mice show profound microglia infiltration and preferential elimination of inhibitory synapses in the ventral thalamus, which lead to hyperexcitability in the thalamocortical circuits and obsessive-compulsive disorder (OCD)-like grooming behaviors. Remarkably, deleting C1qa gene significantly reduces synaptic pruning by $Grn^{-/-}$ microglia and mitigates neurodegeneration, behavioral phenotypes, and premature mortality in $Grn^{-/-}$ mice. Together, our results uncover a previously unrecognized role of progranulin in suppressing aberrant microglia activation during aging. These results represent an important conceptual advance that complement activation and microglia-mediated synaptic pruning are major drivers, rather than consequences, of neurodegeneration caused by progranulin deficiency.

INTRODUCTION

Microglia are innate immune cells that repair injury and maintain homeostasis in the CNS (Ransohoff and Perry, 2009). Previous studies indicate that microglia employ a diverse repertoire of proteins in the innate immune system to regulate synapse formation and maintenance. For example, in early postnatal life, microglia use the classical complement pathway to regulate synapse development in the lateral geniculate nucleus (Schafer et al., 2012; Stevens et al., 2007). During the aging process, however, progressive accumulation of complement C1qa in the dentate gyrus of hippocampus promotes cognitive decline and memory impairments (Stephan et al., 2013). In contrast, loss of complement C3 protein protects against age-dependent declines in synaptic and dendritic spine density in the CA3 region of the

CrossMark

hippocampus and rescues attenuation of long-term potentiation (LTP) (Shi et al., 2015). In addition, microglia also use fractalkine receptor CX3CR1 to regulate the growth and maintenance of dendritic spines on hippocampal neurons, which in turn serve as the structural basis of synapse formation (Paolicelli et al., 2011). Finally, genetic ablation of microglia in the adult brain further reveals the essential role of microglia in the maintenance of synaptic functions and motor learning (Parkhurst et al., 2013). Given these results, it has been proposed that excessive microglial activation may contribute to the pathogenesis of neurodegenerative diseases (Aguzzi et al., 2013). However, whether microglial activation directly contributes to neurodegeneration remains unclear.

In this study, we investigate the role of aberrant microglial activation as the primary pathogenic factor for frontotemporal dementia (FTD), the second most common dementia affecting patients younger than 65 years of age (Rascovsky et al., 2011; Ratnavalli et al., 2002). We focus on the autosomal dominant mutations in the human *progranulin* (*GRN*) gene, which cause a drastic reduction in progranulin (PGRN) levels, contributing to the pathogenesis of one the most common forms of familial frontotemporal lobar degeneration (FTLD) (Baker et al., 2006; Cruts et al., 2006; Finch et al., 2009; Ghidoni et al., 2008; Sleegers et al., 2009). Several studies indicate that PGRN is a key regulator of inflammation and that PGRN deficiency causes an aberrant increase in phagocytosis and pro-inflammatory cytokine production in microglia and macrophages (Kao et al., 2011; Martens et al., 2012; Yin et al., 2010). Furthermore, when exposed to the neurotoxin MPTP, both global *Grn* knockout (*Grn*$^{-/-}$) and microglia-specific *Grn* knockout (*Cd11b-Cre;Grn*$^{fl/fl}$) mutant mice show a much more robust increase in microglial activation and neuronal loss (Martens et al., 2012), supporting the idea that PGRN is required to suppress excessive microglial activation. Finally, rare homozygous *GRN* mutations in humans have been shown to cause neuronal ceroid lipofuscinosis (NCL), which shares similar neuropathological features with FTLD patients with *GRN* mutations (Götzl et al., 2014; Smith et al., 2012). The connection between FTLD caused by *GRN* mutations and NCL is intriguing because neuroinflammation is a prominent and consistent feature in animal models of NCL and lysosomal storage diseases (Castaneda et al., 2008; Cotman et al., 2013). Together, these data suggest that PGRN deficiency may lead to a spectrum of neurodegenerative conditions in a dose-dependent manner.

Despite evidence supporting the role of PGRN in microglia function, it remains unclear how PGRN deficiency causes microglia activation and how PGRN-deficient microglia contribute to neurodegeneration in the aging brain. It is equally unclear whether blocking microglia activation in chronic PGRN deficiency could mitigate neurodegeneration. Here, we show that loss of PGRN causes an age-dependent upregulation of lysosomal and innate immunity genes in microglia, which increases complement production and synaptic pruning activity by microglia to preferentially eliminate inhibitory synapses in the ventral thalamus. These defects lead to hyperexcitability in the thalamocortical circuits and obsessive-compulsive disorder (OCD)-like grooming behaviors. Remarkably, blocking complement activation significantly re-

duces synaptic pruning by *Grn*$^{-/-}$ microglia and mitigates neurodegeneration, behavioral phenotypes, and premature mortality in *Grn*$^{-/-}$ mice. These results uncover a previously unrecognized role of PGRN in suppressing microglia activation and support an important conceptual advance that complement activation and microglia activation are major drivers, rather than consequences, of neurodegeneration caused by PGRN deficiency.

RESULTS

Transcriptional Profiling Reveals Age-Dependent Lysosomal and Innate Immunity Defects in *Grn*$^{-/-}$ Microglia

To investigate how PGRN deficiency contributes to neurodegeneration during aging, we analyzed the transcriptomes of the cerebral cortex, hippocampus, and cerebellum in 2-, 6-, 9-, 12-, and 18-month-old *Grn*$^{+/+}$, *Grn*$^{+/-}$, and *Grn*$^{-/-}$ mice. We used weighted correlation network analysis (WGCNA) to identify highly correlated gene modules that were either up- or downregulated in an age-dependent and genotype-specific manner (Figure 1A) (Langfelder and Horvath, 2008; Zhang and Horvath, 2005). Principal component analyses showed no difference in the transcriptomes between *Grn*$^{+/+}$ and *Grn*$^{+/-}$ brain regions, but revealed an age-dependent upregulation of one particular gene module in the cerebral cortex (magenta module) (Figure 1B), hippocampus (purple module), and cerebellum (pink module) of *Grn*$^{-/-}$ mice (Figure S1A). DAVID gene ontology (GO) analyses of these modules revealed two major categories, the lytic vacuole genes in the lysosomal pathway and genes related to innate immune responses (Table S1). Compared to an independent cell-type enrichment dataset (Zhang et al., 2014), genes in the magenta module (cerebral cortex) showed exclusive association with the microglial lineage (p = 6.52 × 10^{-14}) (Figure 1C, inset). System-level analyses of the top 40 genes from magenta, purple, and pink modules revealed extensive topographical overlap (Figures 1C, S1B, and S1C), supporting functional interactions among these genes. At the center of this interconnected network were complement genes (*C1qa*, *C1qb*, *C1qc*, and *C3*), *CD68*, and *Trem2*, which have been implicated in innate immunity, lysosomal function, and microglial activation (Wang et al., 2015), respectively. These results are consistent with the cell-type enrichment transcriptome data, which shows that *Grn* mRNA is >50-fold enriched in microglia (>881.4 fragments per kilobase of exon per million fragments mapped [FPKM]) (Figure S1D) (Zhang et al., 2014) and support that microglia contribute to the age-dependent transcriptional upregulation of lysosomal and innate immunity genes in the aging *Grn*$^{-/-}$ brain.

To validate the brain region-specific transcriptome profiling results, we isolated microglia from 4- and 16-month-old *Grn*$^{+/+}$ and *Grn*$^{-/-}$ mice using Percoll gradients and fluorescence-activated cell sorting (FACS) with microglia/macrophage/neutrophil markers, CD11b PE, CD45 APC, and anti-Ly6G PE-Cy7 (Figure 1D). This approach revealed a 4-fold increase in the relative abundance of microglia (defined as CD45^{lo};CD11b$^+$, pink gate in Figures 1E and 1F) in 16-month-old *Grn*$^{-/-}$ mice but no detectable increase in macrophage number (defined as
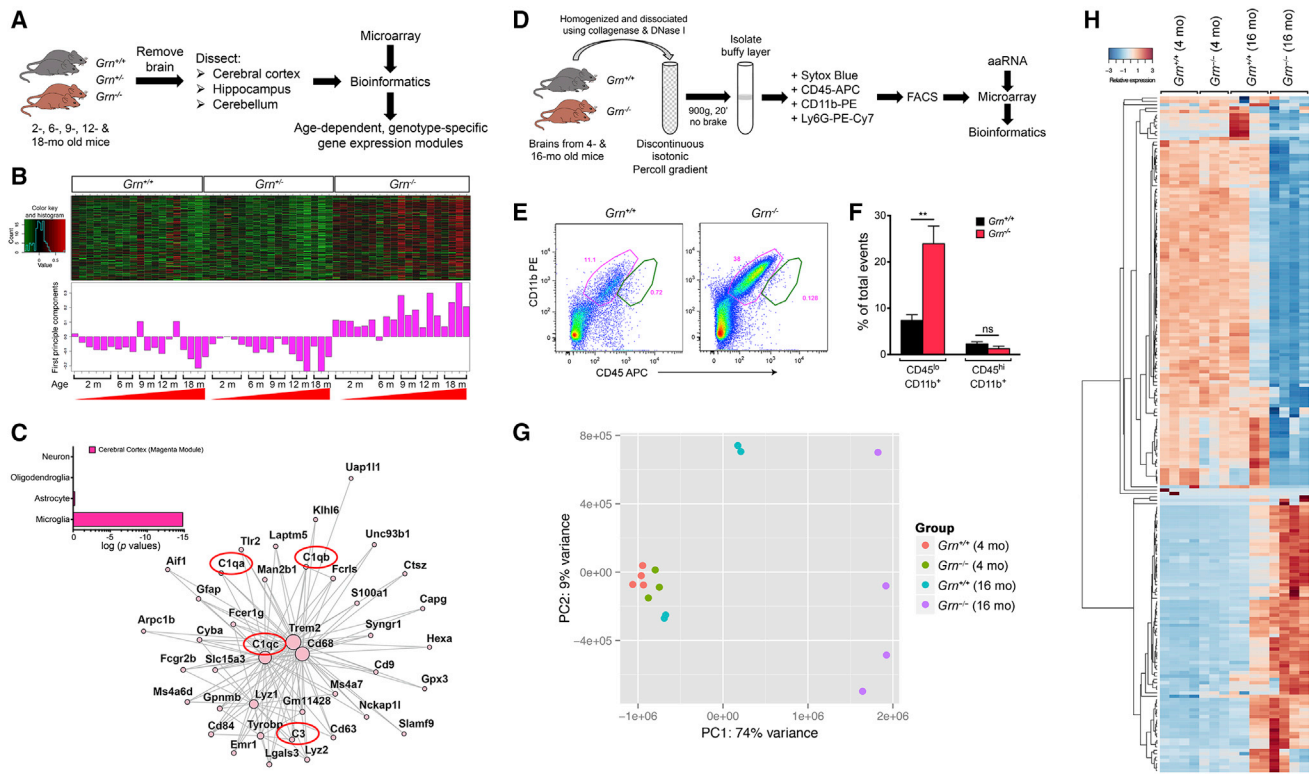
Figure 1. Transcriptome Profiling in $Grn^{+/+}$, $Grn^{+/-}$, and $Grn^{-/-}$ Mice Reveal Age-Dependent Upregulation of Lysosomal and Innate Immunity Genes in Microglia

(A) Diagram showing the procedures to characterize the transcriptomes of specific brain regions in $Grn^{+/+}$, $Grn^{+/-}$, and $Grn^{-/-}$ mice during aging.

(B) Weighted correlation network analysis (WGCNA) identifies highly correlated gene modules that are age-dependently upregulated in the cerebral cortex of $Grn^{-/-}$ mice.

(C) The top 40 genes from the magenta (cerebral cortex) module are highly enriched with microglial genes (inset), and there is extensive topographical overlap among their expression patterns, especially for complements $C1qa$, $C1qb$, $C1qc$ and $C3$, $Cd68$, and $Trem2$.

(D) Diagram showing the procedures to isolate microglia from 4- and 16-month-old $Grn^{+/+}$ and $Grn^{-/-}$ mice using discontinuous isotonic Percoll gradient, FACS, preparation of amplified antisense RNA (aaRNA), microarray, and bioinformatics analyses.

(E) Dissociated cells from 16-month-old $Grn^{+/+}$ and $Grn^{-/-}$ mice are incubated with CD11b PE (clone M1/70) (Invitrogen), CD45 APC (clone Ly5) (eBioscience), and anti-Ly6G PE-Cy7 (clone 1A8) (BD Biosciences), and sorted by Beckman-Coulter MoFlo XDPs flow cytometer.

(F) Microglia are defined as CD45^{lo};CD11b^{+}, whereas macrophages are defined as CD45^{hi};CD11b^{+} population in FACS. Data are presented as % of total events. Student's t test, n = 3 for $Grn^{+/+}$ and $Grn^{-/-}$ mice. **p < 0.01; ns, not significant.

(G) Principle component analysis of the top 500 most variable transcripts from the FACS-sorted microglia from 4- and 16-month-old $Grn^{+/+}$ and $Grn^{-/-}$ mice.

(H) Hierarchical clustering analyses of the top 200 transcripts from FACS-sorted microglia from 4- and 16-month-old $Grn^{+/+}$ and $Grn^{-/-}$ mice.

See also Figure S1 and Table S1.

CD45^{hi};CD11b^{+};Ly6G^{-}, green gate in Figure 1E). We then analyzed the transcriptional profiles of FACS-sorted 4- and 16-month-old $Grn^{+/+}$ and $Grn^{-/-}$ microglia using principle component analysis of the top 500 most variable transcripts and showed that the 4-month-old $Grn^{+/+}$ and $Grn^{-/-}$ microglia replicates clustered closely, suggesting that loss of PGRN had only modest effects on the transcriptional profiles of microglia at this age (Figure 1G). In contrast, 16-month-old $Grn^{-/-}$ microglia showed much more profound alterations in transcriptional profiles than 16-month-old $Grn^{+/+}$ microglia (Figure 1G). Hierarchical clustering analyses of the top 200 transcripts confirmed that the transcriptional profiles of $Grn^{+/+}$ and $Grn^{-/-}$ microglia were similar at 4 months old, but became drastically different at 16 months old (Figure 1H). Together, these results support that PGRN is required to suppress aberrant microglial activation during aging.

Characterizations of PGRN in the Endolysosomal Pathway in Microglia

To characterize how microglia contribute to the upregulation of lysosomal and innate immune response genes in $Grn^{-/-}$ brain, we analyzed lysosomal morphology in the microglia of 4- and 18-month-old $Grn^{+/+}$ and $Grn^{-/-}$ brains. Using CD68 as a marker for lysosomes and Iba-1 for microglia, we found that $Grn^{-/-}$ microglia showed a marked increase in lysosomal size at 18 months old (Figures 2A–2E). Although microglia in 4-month-old $Grn^{+/+}$ and $Grn^{-/-}$ brains showed no difference in the lysosomal size, treatment with neurotoxin 1-methyl-4-phenyl-1,2,3,6-tetrahydropyridine (MPTP) induced a significant increase in the size of CD68^{+} lysosomes in $Grn^{-/-}$ microglia (Figure 2E). Similar MPTP-induced increase in lysosomal size was also detected in the microglia of $Cd11b$-Cre;$Grn^{f/f}$ mutants, suggesting that the
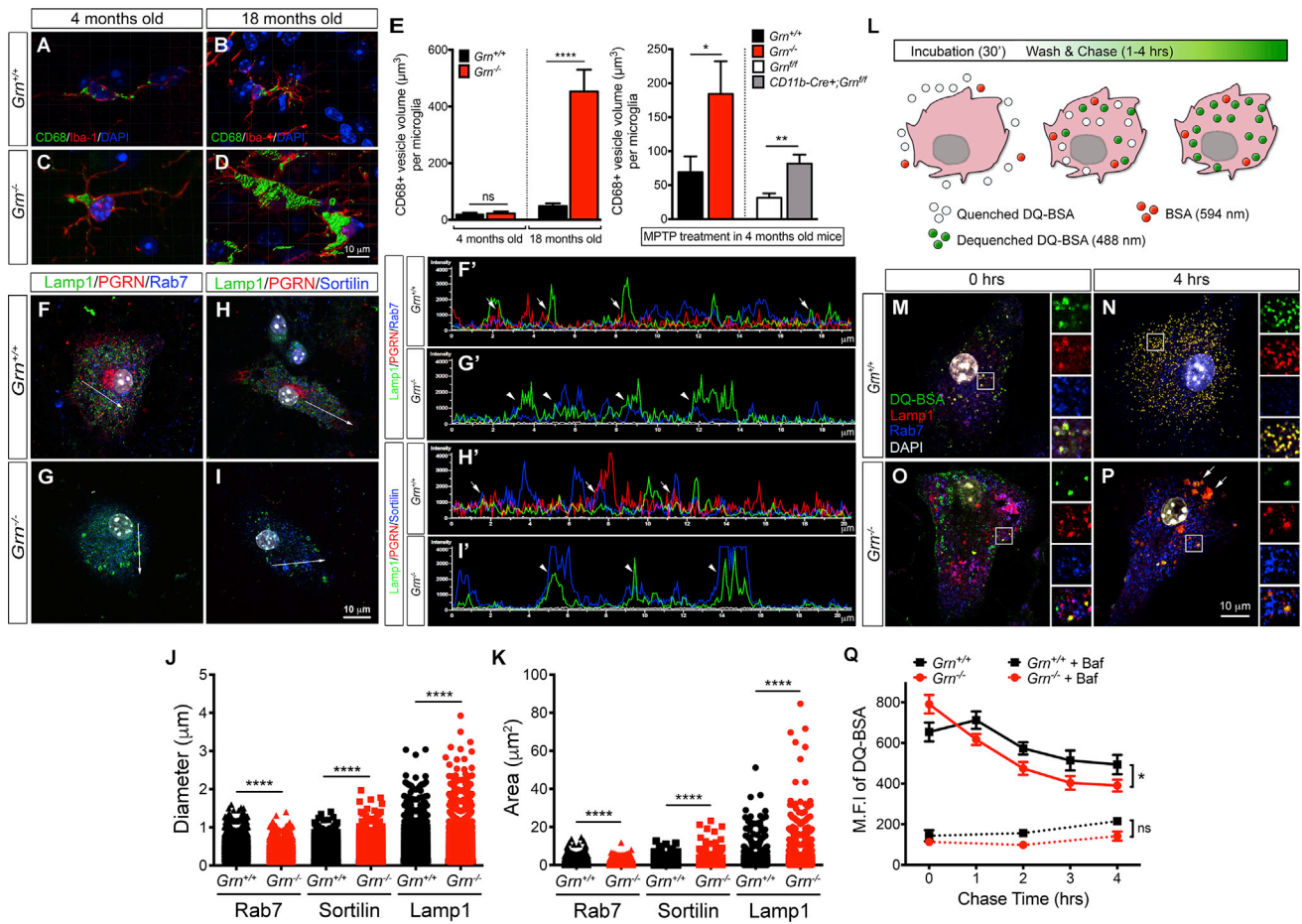
Figure 2. Lysosomal Defects and Increased Complement Production by *Grn*$^{-/-}$ Microglia

(A–D) Confocal images of Iba-1$^+$ microglia from the ventral thalamus of 4- and 18-month-old *Grn*$^{+/+}$ (A and B) and *Grn*$^{-/-}$ (C and D) brains show CD68$^+$ lysosomes in the cytoplasm. Images were captured from *Grn*$^{+/+}$ and *Grn*$^{-/-}$ brains (n = 3 per age) and processed for 3D reconstruction of the lysosomes using Imaris software.

(E) Quantification of CD68$^+$ lysosome volume in the ventral thalamus of 4- and 18-month-old *Grn*$^{+/+}$ and *Grn*$^{-/-}$ mouse brains (left panel) and in 4-month-old *Grn*$^{+/+}$ and *Grn*$^{-/-}$ mouse brains after MPTP treatment (right panel). Volumes are expressed as μm^3 per microglia. Student's t test, n = 3 per group. *p < 0.05, **p < 0.01, ****p < 0.001.

(F–I) Confocal images of primary microglia from neonatal *Grn*$^{+/+}$ (F and H) and *Grn*$^{-/-}$ (G and I) mouse brains that have been co-cultured with wild type cortical neurons. Microglia are labeled with antibodies for Lamp1/PGRN/Rab7 (F and G) or Lamp1/PGRN/Sortilin (H and I). Arrows indicate regions in each microglia where fluorescent signal intensity plots are obtained using Nikon NIS-Elements.

(F′–I′) Fluorescent signal intensity plots of Lamp1$^+$ (green), PGRN$^+$ (red), Rab7$^+$ (blue) (F′ and G′), and Sortilin$^+$ (blue) (H′ and I′) vesicles in *Grn*$^{+/+}$ and *Grn*$^{-/-}$ microglia. Arrows in (F′) and (H′) indicate partial overlap of Lamp1$^+$;PGRN$^+$ or PGRN$^+$;Sortilin$^+$ signals, respectively.

(J and K) Quantification of the size, including diameter (J) and area (K), of Lamp1$^+$, Sortilin$^+$, and Rab7$^+$ vesicles in *Grn*$^{+/+}$ and *Grn*$^{-/-}$ microglia. Student's t test, ****p < 0.001.

(L) Diagram showing DQ-BSA assays in cultured microglia. Open circles are quenched DQ-BSA, green circles are dequenched DQ-BSA, and red circles are BSA-conjugated with 568 nm fluorophore.

(M–P) Representative images of *Grn*$^{+/+}$ (M and N) and *Grn*$^{-/-}$ (O and P) microglia after 30′ incubation with DQ-BSA (0 hr) or 4 hr after washing (4 hr). Scale bar in (P) is 10 μm. Insets to the right of each panel represent enlarged images in the boxed area in (M)–(P). Arrows in (P) indicate dequenched DQ-BSA signals in Lamp1$^+$ lysosomes.

(Q) Quantification of the maximal fluorescence intensity (M.F.I.) of dequenched DQ-BSA in *Grn*$^{+/+}$ (n = 5) and *Grn*$^{-/-}$ microglia (n = 7). Bafilomycin inhibits lysosomal acidification and protein degradation in *Grn*$^{+/+}$ and *Grn*$^{-/-}$ microglia. Two-way ANOVA, *p < 0.05.

See also Figure S2.

lysosomal defects in *Grn*$^{-/-}$ microglia may be tightly coupled to their activation state.

To further characterize the lysosomal defects in *Grn*$^{-/-}$ microglia, we examined the subcellular localization of PGRN and the effects of PGRN deletion on lysosome morphology. Using confocal microscopy and fluorescent signal intensity plots of PGRN and markers for early endosomes (Rab5), late endosomes (Rab7), *trans*-Golgi network (Sortilin), and early lysosomes (Lamp1), we showed that PGRN did not co-localize with Rab5$^+$ vesicles in *Grn*$^{+/+}$ microglia (data not shown), but was detected

in Golgi apparatus and in vesicles that were immediately adjacent to and partially overlapped with Rab7$^+$, Sortilin$^+$, and Lamp1$^+$ vesicles (Figures 2F, 2F', 2H, 2H', arrows, and S2). In contrast, Grn$^{-/-}$ microglia showed many enlarged Lamp1$^+$ vesicles that co-expressed Rab7 or Sortilin (Figures 2G, 2G', 2I, 2I', arrowheads, and S2). Quantification using NIH ImageJ further revealed that Rab7$^+$ vesicles were modestly reduced in size in Grn$^{-/-}$ microglia, whereas the size of Lamp1$^+$ or Sortilin$^+$ vesicles was significantly increased (Figures 2J, 2K, and S2).

Given the phagocytic activity of microglia, we asked whether loss of PGRN might alter endolysosomal functions. To this end, we incubated Grn$^{+/+}$ and Grn$^{-/-}$ microglia with BSA conjugated with fluorophore that emitted signal at 594 nm for 30' and found no difference in Grn$^{+/+}$ and Grn$^{-/-}$ microglia to endocytose BSA (data not shown). We then incubated Grn$^{+/+}$ and Grn$^{-/-}$ microglia with a green BODIPY dye conjugated to BSA (DQ-BSA) (10 μg/ml), which upon proteolysis in acidic lysosomal compartments becomes dequenched and releases bright fluorescent signals (Figure 2L) (Vázquez and Colombo, 2009). After incubation with DQ-BSA for 30', the intracellular trafficking of dequenched DQ-BSA signals in microglia were monitored using confocal microscopy and flow cytometry at 0, 1, 2, 3, and 4 hr. At the end of 30' incubation, Grn$^{-/-}$ microglia contained ∼20% more dequenched DQ-BSA than Grn$^{+/+}$ microglia, most were located in Lamp1$^+$ and Rab7$^+$ vesicles (Figures 2M, 2O, and 2Q). Interestingly, 4 hr after washing, Grn$^{+/+}$ microglia still retained >75% of the dequenched DQ-BSA signals within the Lamp1$^+$ vesicles (Figures 2N and 2Q). In contrast, only 49.3% of dequenched DQ-BSA signals remained in Lamp1$^+$ vesicles in Grn$^{-/-}$ microglia (Figures 2P and 2Q). These results indicate that Grn$^{-/-}$ microglia are more efficient in processing materials via the endolysosomal pathway. To further demonstrate that the lysosomal functions in Grn$^{-/-}$ microglia are indeed intact, we used bafilomycin A1 (5 nM), a vacuolar type H$^+$-ATPase inhibitor, to block acidification and protein degradation in lysosomes (Yoshimori et al., 1991). This treatment completely blocked DQ-BSA signals in Grn$^{+/+}$ and Grn$^{-/-}$ microglia with no detectable differences (Figure 2Q).

Complement Protein C1qa Promotes Synaptic Pruning by Grn$^{-/-}$ Microglia
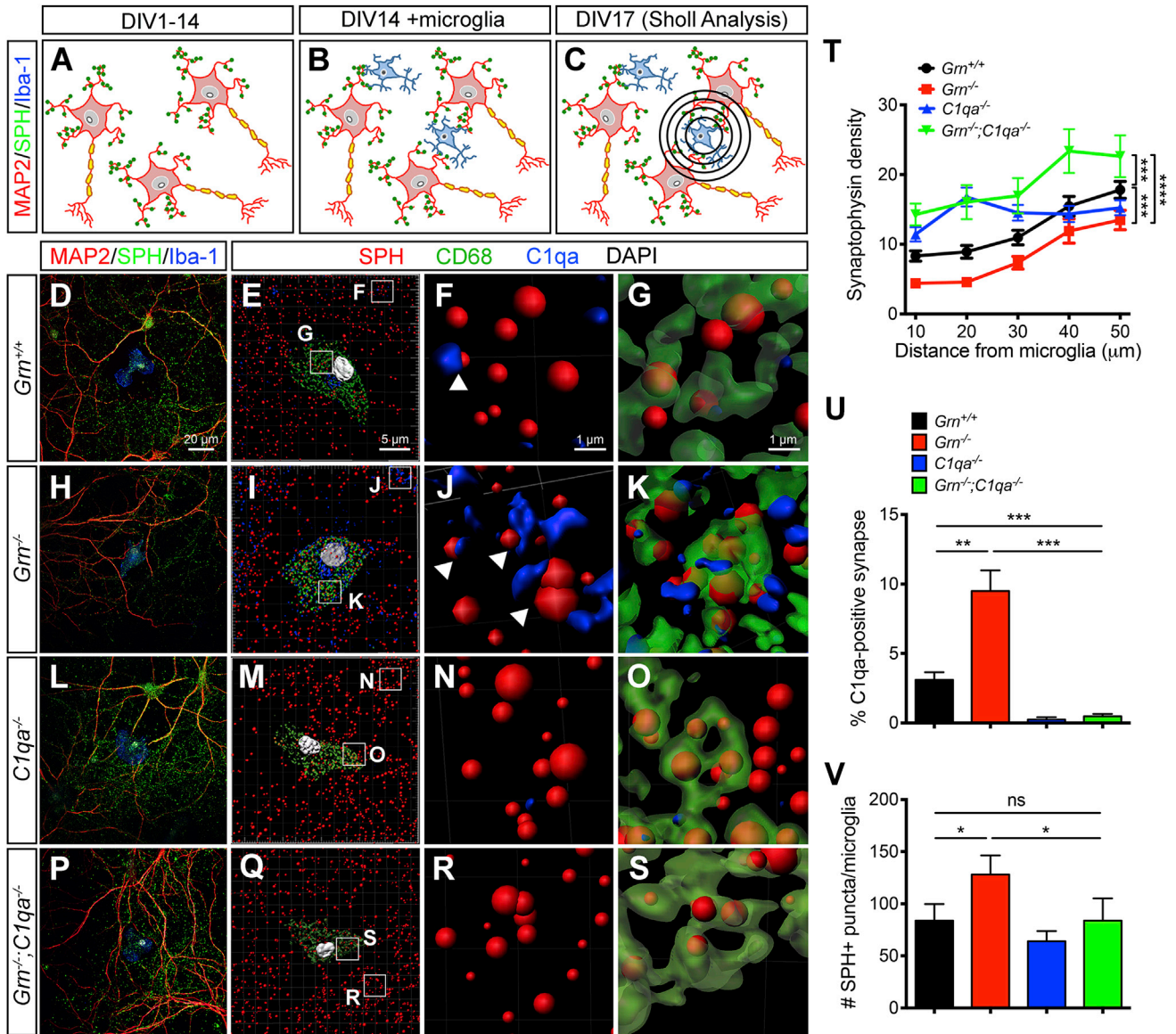
To investigate the functional consequences of the lysosomal defects in Grn$^{-/-}$ microglia, we asked whether this phenotype promotes activation of innate immunity and thereby promoting neurodegeneration. Among the innate immune response genes upregulated in Grn$^{-/-}$ brain, we focused on the complement system because complement-mediated synaptic pruning is a key mechanism in modulating neural circuit functions (Schafer et al., 2012; Stephan et al., 2013; Stevens et al., 2007). Furthermore, aberrant lysosome-mediated cleavage of complement protein C3 induces proinflammatory cytokine production in T lymphocytes and contributes to the pathogenesis of autoimmune disease (Liszewski et al., 2013). To characterize the role of complements in PGRN deficiency, we performed qRT-PCR using mRNA from Grn$^{+/+}$ and Grn$^{-/-}$ primary cortical neurons and neonatal microglia and showed that C1qa and C3 mRNA levels were much more abundant in Grn$^{-/-}$ microglia and further upregulated upon treatment with lipopolysaccharide (LPS) (Fig-

ures S3A and S3B). FACS analyses using antibodies specific for C1qa, C3, and C3b confirmed more abundant complements in primary microglia from neonatal Grn$^{-/-}$ mouse brain in regular culture conditions and upon LPS treatment (Figures S3C and S3D). Finally, confocal microscopy showed that Grn$^{-/-}$ microglia acutely isolated from neonatal Grn$^{-/-}$ mouse brains expressed abundant C3 proteins that co-localized with lysosomal marker Lamp1 and secretory marker Grasp55 (Figures S3E–S3H), supporting that C3 proteins are processed in the lysosomes and released via the secretory pathway. In addition, microglia in 12-month-old Grn$^{-/-}$ brains contained abundant C1qa in the cytoplasm, whereas microglia in Grn$^{+/+}$ brains had very low C1qa expression (Figures S3I–S3N).

Given the marked increases in C1qa and C3 in Grn$^{-/-}$ microglia, we reasoned that increased complement production and upregulation of lysosomal genes might allow Grn$^{-/-}$ microglia to be more efficient in pruning synapses. To test this, we designed a co-culture system in which wild-type cortical neurons were plated at low density to allow uniform synapse development for 14 days in vitro (DIV14) (Figure 3A). Concurrently, microglia were cultured from Grn$^{+/+}$ and Grn$^{-/-}$ neonatal brains and added to cortical neurons at 1:3 ratio at DIV14. The co-cultures continued for 3 more days before they were collected for immunostaining and analysis (Figures 3B and 3C). To show the effect of microglia in synaptic pruning, we used a modified Sholl analysis to quantify the amount synaptophysin$^+$ synapses around the cell body of microglia (Figure 3C). We also used the Imaris software to perform 3D reconstruction of confocal images to quantify the number of C1qa-tagged synapses and the number of synapses within the lysosomes of microglia.

In Grn$^{+/+}$ microglia-neuron co-cultures, the synaptic density adjacent to the cell body of microglia was low, with progressive increase in areas distant from microglia (Figures 3D and 3T, black line). Approximately 3% of synapses in Grn$^{+/+}$ microglia-neuron co-cultures were immediately adjacent to C1qa-positive signals (Figures 3E and 3F), suggesting that these synapses were "tagged" by C1qa for removal. Indeed, several synapses were identified in CD68$^+$ lysosomes within the cytoplasm of Grn$^{+/+}$ microglia (Figure 3G). In contrast, the synaptic density surrounding Grn$^{-/-}$ microglia was significantly lower than that around Grn$^{+/+}$ microglia (Figures 3H and 3T, red line). Furthermore, there were more C1qa-positive synapses both outside Grn$^{-/-}$ microglia and within the CD68$^+$ lysosomes inside Grn$^{-/-}$ microglia (Figures 3I–3K and 3T–3V).

In C1qa$^{-/-}$ microglia-neuron co-cultures, the synaptic density around microglia was much higher, especially within a 30-μm radius (Figures 3L, 3M, and 3T, blue line). No C1qa was detected near or within the synapse, again supporting the idea that C1qa was made by microglia, not by neurons (Figures 3N and 3U). The number of synapse within CD68$^+$ lysosomes in C1qa$^{-/-}$ microglia was also significantly lower than that in Grn$^{-/-}$ microglia (Figures 3O and 3V), indicating that loss of C1qa reduced the synaptic pruning activity of microglia. To determine if loss of C1qa could mitigate synaptic pruning by Grn$^{-/-}$ microglia, we performed microglia-neuron co-cultures using microglia from Grn$^{-/-}$;C1qa$^{-/-}$ neonatal mice and showed that the synaptic density around Grn$^{-/-}$;C1qa$^{-/-}$ microglia was indeed much

Figure 3. Increased Synaptic Pruning Activity in *Grn*$^{-/-}$ Microglia Requires C1qa

(A–C) Diagrams showing microglia-neuron co-cultures (A and B) and Sholl (C) analyses to quantify synapses around microglia.

(D–S) Confocal images showing the presence of synapses (SPH$^+$) around *Grn*$^{+/+}$, *Grn*$^{-/-}$, *C1qa*$^{-/-}$, and *Grn*$^{-/-}$;*C1qa*$^{-/-}$ microglia (Iba1$^+$) (D, H, L, and P). Imaris 3D image reconstruction of the microglia-neuron co-cultures at a lower magnification (E, I, M, and Q). Higher magnification shows the presence of C1qa immediately adjacent synapses (F, J, N, R) and C1qa-tagged synapses inside CD68$^+$ lysosomes in microglia (G, K, O, and S). Scale bar, 20 μm (D); 5 μm (E); 1 μm (F and G).

(T) Synaptic density around *Grn*$^{+/+}$, *Grn*$^{-/-}$, *C1qa*$^{-/-}$, and *Grn*$^{-/-}$;*C1qa*$^{-/-}$ microglia. ***p < 0.005, ****p < 0.001, two-way ANOVA, n = 4 for all genotypes.

(U and V) Quantification of the percentage of C1qa-tagged synapses outside microglia (U) and the number of SPH$^+$ synapse inside microglia (V). *p < 0.05, **p < 0.01, ***p < 0.005, Student's t test, n = 4 per genotype.

See also Figure S3.

higher compared to that in *Grn*$^{-/-}$ and *Grn*$^{+/+}$ microglia-neuron co-cultures (Figures 3P and 3T, green line). Similar to the results from *C1qa*$^{-/-}$ microglia, no C1qa was detected near or at the synapse in *Grn*$^{-/-}$;*C1qa*$^{-/-}$ microglia-neuron co-cultures, and the number of synapses within the lysosomes of *Grn*$^{-/-}$;*C1qa*$^{-/-}$ microglia was also reduced (Figures 3R–3V). Together, these results support that the increase of C1qa in *Grn*$^{-/-}$ microglia pro-

motes, whereas loss of C1qa in *Grn*$^{-/-}$;*C1qa*$^{-/-}$ microglia reduces synaptic pruning activity.

Age-Dependent Complement Activation at the *Grn*$^{-/-}$ Thalamic Synapses

Having observed the increased synaptic pruning activity in *Grn*$^{-/-}$ microglia, we asked whether specific regions in *Grn*$^{-/-}$

mouse brains are more severely affected by the increases in complements and microglia and how this might contribute to neurodegeneration. To test this, we performed qRT-PCR using mRNA from cerebral cortex, hippocampus, caudate/putamen, cerebellum, and thalamus from 12-month-old $Grn^{+/+}$ and $Grn^{-/-}$ brains and showed that $C1qa$ and $C3$ mRNA were most abundant in the thalamus in $Grn^{-/-}$ brains, with an age-dependent increase (Figures 4A–4D). In addition, western blots showed that both C1qa and C3 cleavage product iC3b were age-dependently upregulated in the thalamus of $Grn^{-/-}$ mice (Figures 4E and 4F).

Given the role of complements in synaptic pruning, we asked whether C1qa and C3 were deposited near or at the synapses in vivo. To address this, we performed immunostains and showed very low C1qa signal in the ventral thalamus of $Grn^{+/+}$ mice at 4 and 18 months old (Figures 4G and 4H). In contrast, C1qa staining intensity showed a modest increase around the ventral thalamic nuclei of $Grn^{-/-}$ mice at 4 months old and a much more prominent increase at 18 months old (Figures 4I and 4J). Whereas no detectable C1qa was found in the cell body of $Grn^{+/+}$ or $Grn^{-/-}$ thalamic neurons, abundant C1qa was found in the neuropil surrounding the cell bodies and processes of $Grn^{-/-}$ neurons (Figures 4K–4P).

To test if C1qa was deposited near or at synapses in the ventral thalamus of $Grn^{-/-}$ brain, we performed double labeling using antibodies for C1qa and the presynaptic marker synaptophysin (SPH). Consistent with our prediction, most C1qa signals were in close proximity to SPH$^+$ puncta in the thalamus of $Grn^{-/-}$ mice. No detectable C1qa signals were found near the synapses in $Grn^{+/+}$ brain (Figures 4Q–4V). In addition, immunogold electron microscopy (IEM) showed that C1qa was immediately adjacent to synapses in $Grn^{-/-}$ thalamus, but not in $Grn^{+/+}$ thalamus (Figures 4W and 4X). Finally, to provide biochemical evidence for complement deposition at the synapses of $Grn^{-/-}$ mice, we used discontinuous sucrose gradient to isolate synaptosomes from 4-, 9-, and 16-month-old $Grn^{+/+}$ and $Grn^{-/-}$ mouse brains (Carlin et al., 1980) and showed an age-dependent increase in C1qa and multiple C3 cleavage products in the synaptosomes from $Grn^{-/-}$ brain (Figure 4Y).

Removing C1qa in $Grn^{-/-};C1qa^{-/-}$ Mice Protects Synapse Loss, Restores Thalamic Microcircuit Function, Mitigates OCD-like Behaviors, and Improves Survival

To determine whether synapse loss is a major phenotype in $Grn^{-/-}$ mouse brain and whether C1qa removal might protect synapse loss, we established an aging cohort of $Grn^{+/+}$, $Grn^{-/-}$, $C1qa^{-/-}$, and $Grn^{-/-};C1qa^{-/-}$ mice and examined microgliosis and synaptic density in the ventral thalamus from 2 to 19 months old. During aging, the number of microglia in the ventral thalamus of $Grn^{+/+}$ and $C1qa^{-/-}$ mice only showed a very modest increase, with inconspicuous cytoplasm and thin, delicate processes, consistent with resting, quiescent microglia morphology (Figures 5A, 5B, 5E, 5F, and 5I). In contrast, $Grn^{-/-}$ mice showed an age-dependent increase in microglia in the ventral thalamus, and the majority of $Grn^{-/-}$ microglia exhibited abundant cytoplasm with short, prominent processes consistent with reactive microglia (Figures 5C, 5D, and 5I). Interestingly, compared to $Grn^{-/-}$ mice, $Grn^{-/-};C1qa^{-/-}$ mice showed a consistent and

significant reduction in the number of microglia in the ventral thalamus at 7, 12, and 19 months old (p = 0.0006, two-way ANOVA) (Figures 5G–5I). Furthermore, $Grn^{-/-};C1qa^{-/-}$ microglia showed mixed morphology similar to $Grn^{+/+}$ or $Grn^{-/-}$ microglia (Figure 5H). Using SPH as a marker for synaptic density, we found no detectable loss of synapse in the ventral thalamus of $Grn^{+/+}$ and $C1qa^{-/-}$ mice during aging (Figures 5J, 5L, and 5N). In contrast, $Grn^{-/-}$ mice showed significant reductions in SPH density in the ventral thalamus at 4, 7, 12, and 19 months old, whereas SPH density in $Grn^{-/-};C1qa^{-/-}$ mice was almost completely preserved (Figures 5K, 5M, and 5N). These results are consistent with data from microglia-neuron co-cultures and support the essential role of C1qa in mediating synaptic pruning by $Grn^{-/-}$ microglia in vivo.

Given the progressive loss of SPH in the ventral thalamus of $Grn^{-/-}$ mice, we asked whether synaptic pruning preferentially affects excitatory or inhibitory synapses. Within the ventral thalamus, neurons in the ventral posterolateral (VPL) and ventral posteromedial (VPM) nuclei project to layer IV of somatosensory cortex and receive excitatory inputs from neurons in layer VI (Figures S4A and S4B). The sole source of inhibition to this reciprocally excitatory circuit comes from parvalbumin-positive (Parv$^+$) inhibitory neurons in the thalamic reticular nuclei (TRN), which co-express vesicular GABA transporter VGAT (Figures 6A, 6A′, and S4C–S4J). To investigate whether C1qa protein deposits in the ventral thalamus of $Grn^{-/-}$ mice can perturb the balance of excitatory and inhibitory synaptic inputs, we used confocal images to show that C1qa proteins extensively surrounded both VGLUT2$^+$ excitatory and VGAT$^+$ inhibitory synapses in the ventral thalamus of $Grn^{-/-}$ mice (Figures S5A–S5D). Although C1qa deposits showed no preference for excitatory or inhibitory synapses, the number of Parv$^+$ synapses in the VPM and VPL of 12-month-old $Grn^{-/-}$ mice was significantly reduced (Figures 6B and 6B′). Many Parv$^+$ synapses were in close proximity to Iba1$^+$ microglial processes, suggesting that $Grn^{-/-}$ microglia were actively pruning these synapses. Similar to these data, the number of VGAT$^+$ synapses also showed significant reduction in the ventral thalamus of $Grn^{-/-}$ mice from 8 to 19 months old (Figures 6E, 6F, and 6I). In contrast, the number of VGAT$^+$ synapses in $Grn^{-/-};C1qa^{-/-}$ mice showed complete preservation (Figures 6G–6I). Remarkably, unlike the VGAT$^+$ synaptic phenotype, the number of VGLUT2$^+$ excitatory synapses showed no reduction in $Grn^{-/-}$, $C1qa^{-/-}$, or $Grn^{-/-};C1qa^{-/-}$ mice (Figures S5E–S5I).

To characterize how loss of inhibitory synapses in the ventral thalamus of $Grn^{-/-}$ mice might alter circuit function, we performed multiunit array extracellular recording in VPM and VPL in freshly prepared brain slices from 12-month-old $Grn^{+/+}$ and $Grn^{-/-}$ mice (Figure 6J). This approach preserves an intact intra-thalamic circuit and has been instrumental in determining the thalamic function in rodents (Paz et al., 2011, 2013). In the ventral thalamus of $Grn^{+/+}$ mice, electrical stimulation of the internal capsule generated occasional bursts of action potentials (AP) (Figure 6K). In contrast, the same stimulation in the ventral thalamus of $Grn^{-/-}$ brain slices evoked a long-lasting and sustained tonic firing, with significant increase in AP firing frequency and the relative probability of eliciting AP (p < 0.0001) (Figure 6L). Remarkably, loss of C1qa in $Grn^{-/-};C1qa^{-/-}$ mice completely reversed the hyperexcitability phenotype observed in the $Grn^{-/-}$
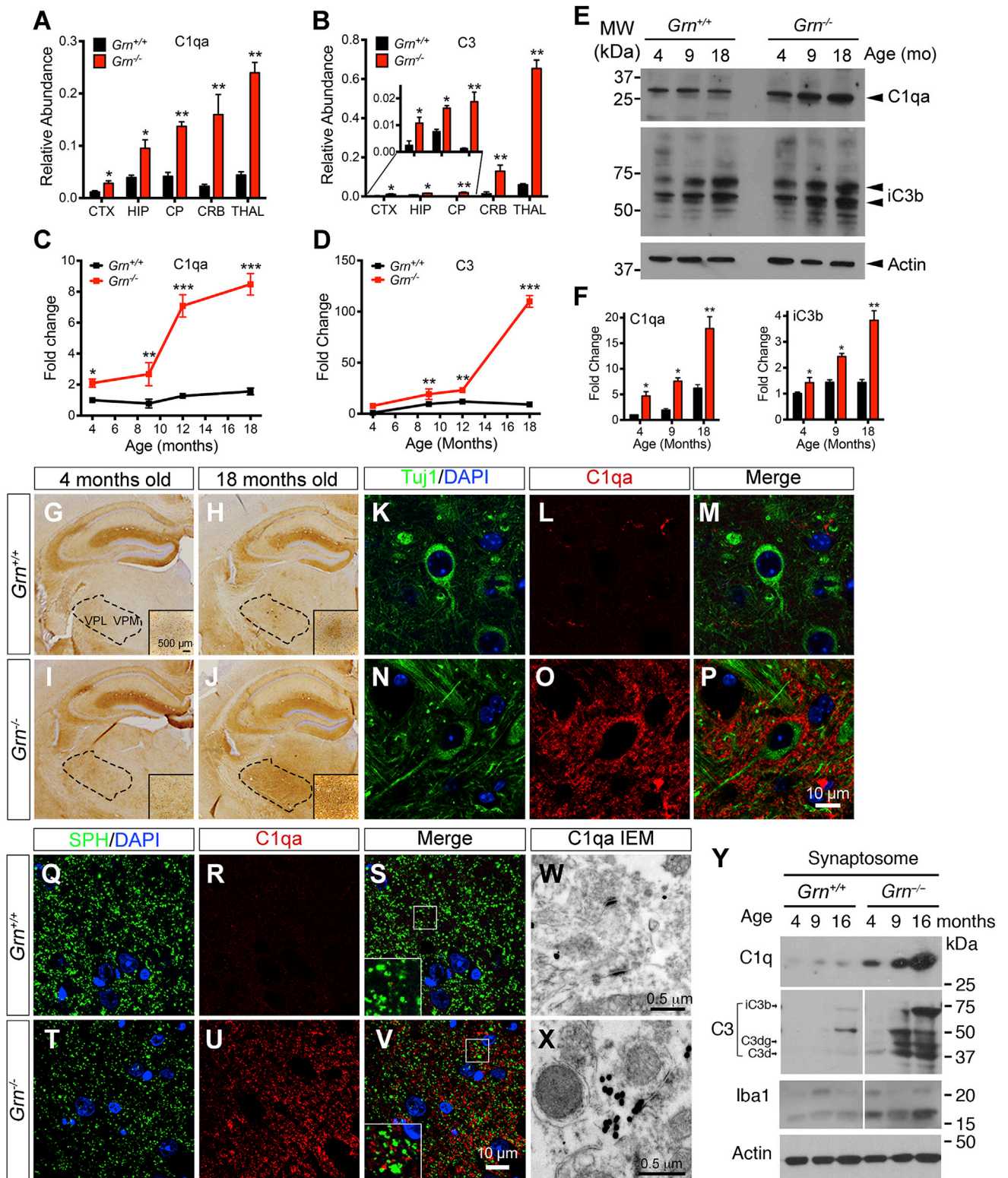
Figure 4. Age-Dependent C1qa Accumulation at the Synapses of the Ventral Thalamus in *Grn*^{−/−} Mice

(A and B) qRT-PCR detects the relative abundance of *C1qa* (A) and *C3* (B) mRNA in cerebral cortex (CTX), hippocampus (HIP), caudate-putamen (CP), cerebellum (CRB), and thalamus (THAL) of 12-month-old *Grn*^{+/+} and *Grn*^{−/−} mice.

(C and D) qRT-PCR shows the progressive increase of *C1qa* (C) and *C3* (D) mRNA in the thalamus of 4-, 9-, 12-, and 18-month-old *Grn*^{−/−} mice.
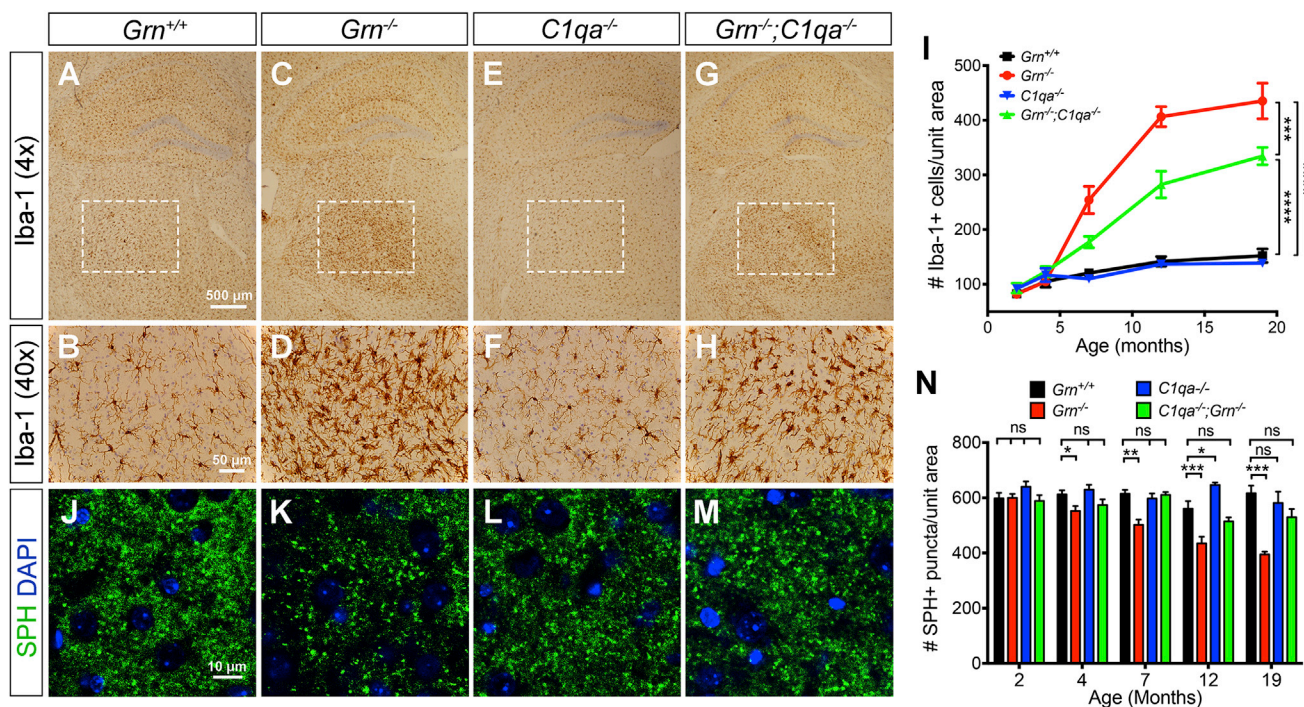
(legend continued on next page)

Figure 5. Reduced Microglia Number and Preservation of Synaptic Density in the Ventral Thalamus of *Grn*$^{-/-}$;*C1qa*$^{-/-}$ Mutant Mice

(A–H) Immunostains for Iba-1 in coronal sections of 12-month-old *Grn*$^{+/+}$ (A and B), *Grn*$^{-/-}$ (C and D), *C1qa*$^{-/-}$ (E and F), and *Grn*$^{-/-}$;*C1qa*$^{-/-}$ (G and H) mouse brains at the level of anterior hippocampus. The square dotted boxes in (A), (C), (E), and (G) highlight the ventral thalamus, where the higher magnification images are obtained. Scale bars, 500 μm (A); 50 μm (B).

(I) Iba-1^{+} microglial density in the ventral thalamus of *Grn*$^{+/+}$, *Grn*$^{-/-}$, *C1qa*$^{-/-}$, and *Grn*$^{-/-}$;*C1qa*$^{-/-}$ mouse brains at 2, 4, 7, 12, and 19 months old. ***p < 0.005, ****p < 0.001, two-way ANOVA, n = 4 per genotype per age.

(J–M) Confocal images of synaptophysin in 12-month-old *Grn*$^{+/+}$ (J), *Grn*$^{-/-}$ (K, *C1qa*$^{-/-}$ (L), and *Grn*$^{-/-}$;*C1qa*$^{-/-}$ (M) brains. Scale bar, 10 μm (J).

(N) Synaptophysin density in *Grn*$^{+/+}$, *Grn*$^{-/-}$, *C1qa*$^{-/-}$, and *Grn*$^{-/-}$;*C1qa*$^{-/-}$ brains at 2, 4, 7, 12, and 19 months old. *p < 0.05, **p < 0.01, ***p < 0.005, ns, not significant. Student's t test, n = 4 per genotype per age.

mice and restored the evoked firing pattern in the thalamus to a pattern similar to *Grn*$^{+/+}$ mice (Figures 6K and 6L).

Dysfunction in the thalamus and striatum has been implicated in obsessive compulsive disorder (OCD), a key clinical feature in FTD (Fitzgerald et al., 2011; Rascovsky et al., 2011). Consistent with hyperexcitability in the ventral thalamus, *Grn*$^{-/-}$ mice exhibited increased grooming activity, consisting of bouts of high-frequency repetitive movement that covered the snout, face, ear, and back (Movie S1). These excessive grooming behaviors began at 8 months old and persisted at 12 months old (Figures 6M and S6A). Due to excessive grooming, >60% of *Grn*$^{-/-}$ mice developed severe skin ulcerations. In addition, ~10% of *Grn*$^{-/-}$ mice also developed motor dysfunction, including unsteady gait and imbalance (Movie S1). These two

phenotypes contributed to the early mortality in *Grn*$^{-/-}$ mice (median survival for *Grn*$^{-/-}$ mice was 529 days, compared to 735 days in *Grn*$^{+/+}$ mice, p < 0.0001, log rank [Mantel-Cox] test) (Figures 6N and 6O). In contrast, *Grn*$^{-/-}$;*C1qa*$^{-/-}$ mice showed significantly reduced grooming activity, more modest skin lesions, and improved survival (Figures 6M–6O and S6B–S6D). These results support that blocking complement activation via *C1qa* gene deletion can mitigate the neurodegenerative phenotypes in *Grn*$^{-/-}$ mice.

Complement Activation as Biomarkers for FTLD with *GRN* Mutations

Finally, we asked whether microglial and complement activation also contribute to neurodegeneration in FTD patients with

(E and F) Western blots (E) and quantification (F) showing the relative abundance of C1qa and C3 proteins in the thalamus of 4-, 9-, and 18-month-old *Grn*$^{+/+}$ and *Grn*$^{-/-}$ mice. *p < 0.05, **p < 0.01, ***p < 0.005, Student's t test. Error bars indicate SEM. n = 3 per age for *Grn*$^{+/+}$ and *Grn*$^{-/-}$ mice.

(G–J) Immunostains in 4- and 18-month-old *Grn*$^{+/+}$ (G and H) and *Grn*$^{-/-}$ (I and J) mouse brain detect C1qa signals in the VPM and VPL thalamic nuclei (dotted areas). Scale bar, 500 μm (G).

(K–P) Confocal images using neuronal marker TuJ1 (K and N) and C1qa (L and O) antibodies in the ventral thalamus of 12-month-old *Grn*$^{+/+}$ and *Grn*$^{-/-}$ mice. (M) and (P) are merged images. Scale bar, 10 μm (P).

(Q–V) Colocalization of synaptophysin (Q and T) and C1qa (R and U) in the ventral thalamus of 12-month-old *Grn*$^{+/+}$ and *Grn*$^{-/-}$ mice. (S) and (V) are merged images. Scale bar, 10 μm (V).

(W and X) Immunogold EM detects C1qa deposits in synapses in the ventral thalamus of 12-month-old *Grn*$^{+/+}$ (W) and *Grn*$^{-/-}$ (X) mice. Scale bars, 0.5 μm.

(Y) Western blots using synaptosomes from 4-, 9-, and 16-month-old *Grn*$^{+/+}$ and *Grn*$^{-/-}$ brains detect C1qa and cleaved C3 proteins.
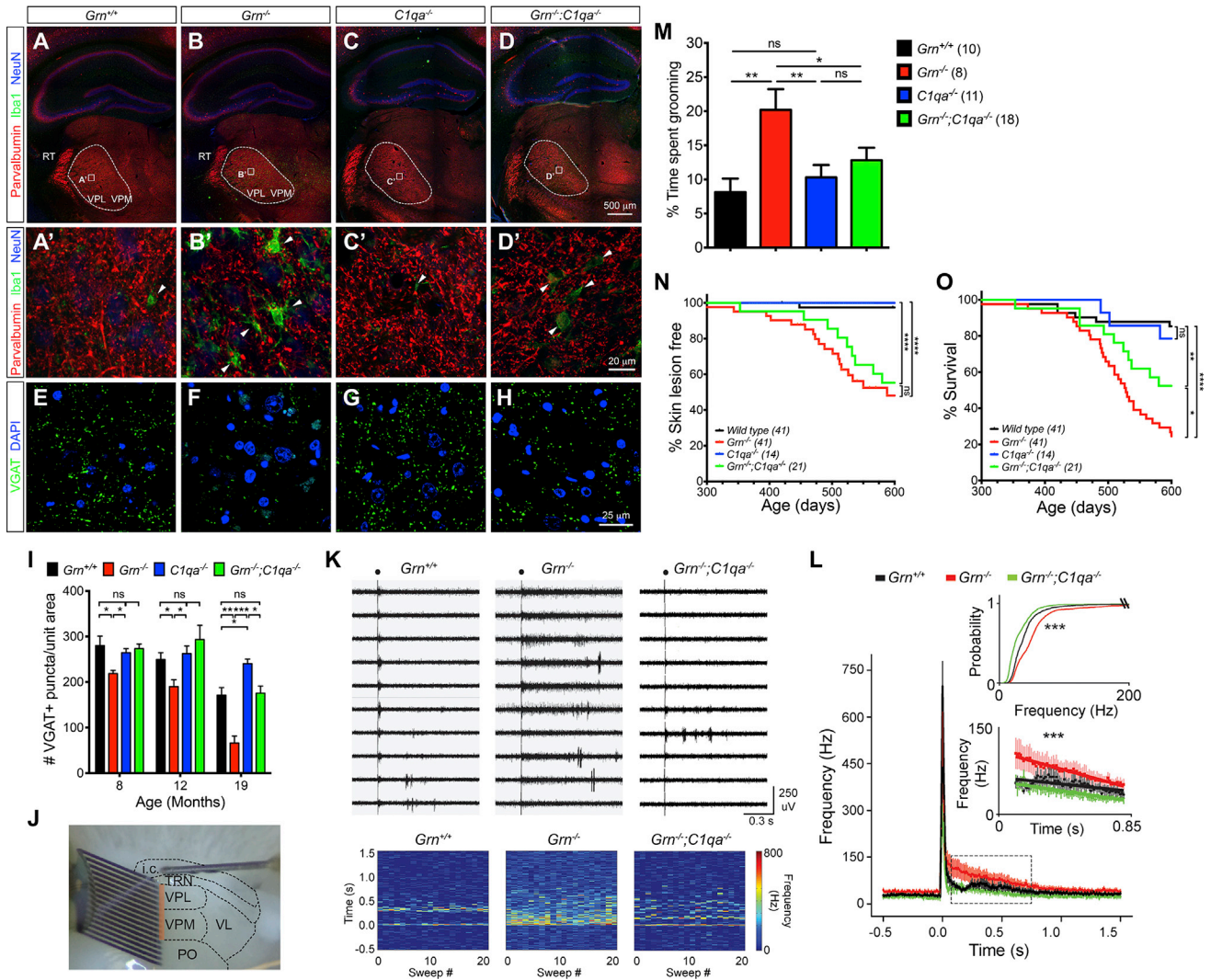
Figure 6. Removing C1qa in $Grn^{-/-};C1qa^{-/-}$ Mice Protects Synaptic Pruning, Restores Thalamic Microcircuit Function, Mitigates OCD-like Behaviors, and Improves Survival

(A–D′) Confocal images of parvalbumin (Parv) show the projection of Parv$^+$ neurons in the reticular nucleus (TRN) to the ventroposterior medial (VPM) and ventroposterior lateral (VPL) nuclei in the ventral thalamus of 12-month-old $Grn^{+/+}$ (A and A′), $Grn^{-/-}$ (B and B′), $C1qa^{-/-}$ (C and C′), and $Grn^{-/-};C1qa^{-/-}$ (D and D′) mice. Dashed lines highlight VPM and VPL nuclei, and squares highlight regions of higher magnification in (A′)–(D′). Scale bars, 500 μm (D); 20 μm (D′).

(E–H) Confocal images of VGAT$^+$ synapses in the ventral thalamus in 19-month-old $Grn^{+/+}$ (E), $Grn^{-/-}$ (F), $C1qa^{-/-}$ (G), and $Grn^{-/-};C1qa^{-/-}$ (H) mice. Scale bar, 25 μm (H).

(I) Quantification of VGAT$^+$ synaptic density in the ventral thalamus of 8-, 12-, and 19-month-old $Grn^{+/+}$, $Grn^{-/-}$, $C1qa^{-/-}$, and $Grn^{-/-};C1qa^{-/-}$ mice. Student's t test, *p < 0.05, **p < 0.01, ***p < 0.005; ns, not significant.

(J) Image of a thalamic slice showing the stimulating electrode in the internal capsule and the 16-channel linear array silicon probe that records multiunit firing in VPM and VPL.
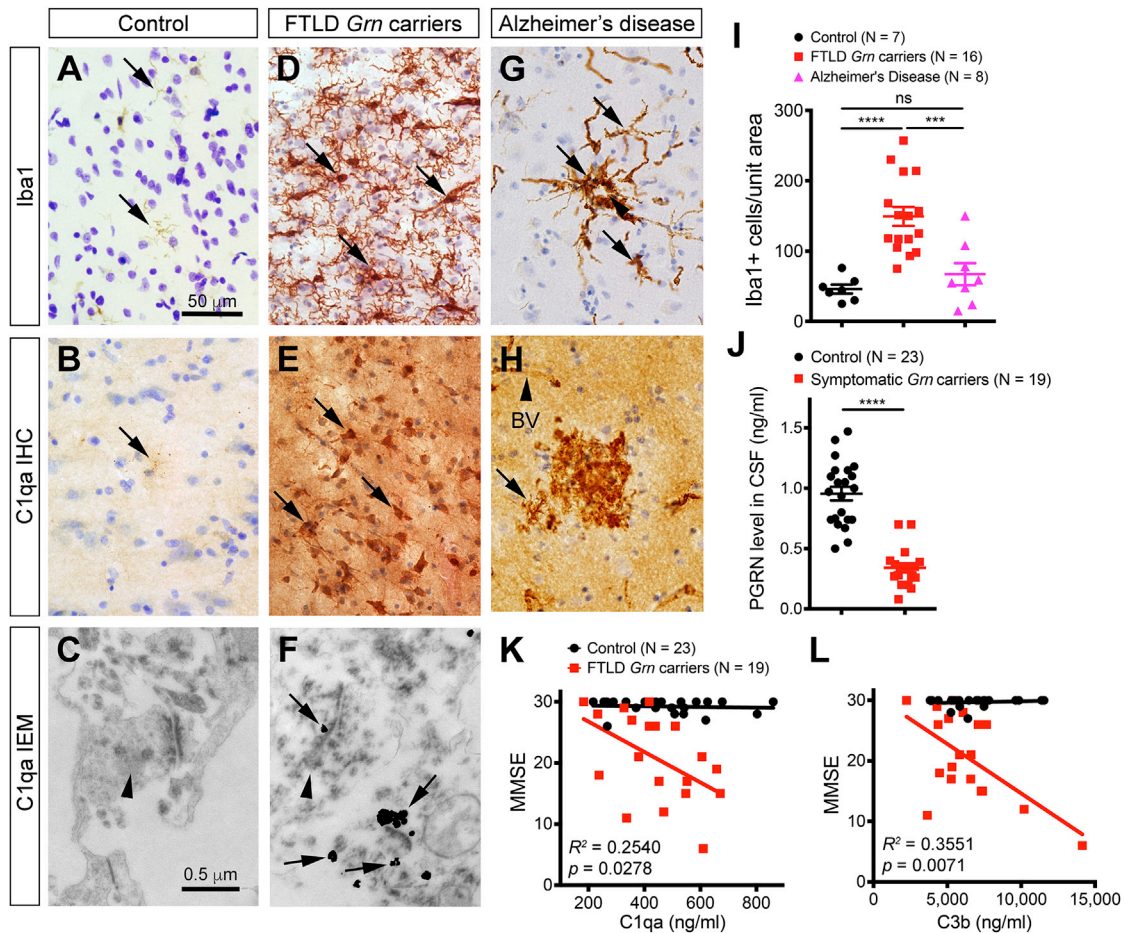
(K) Representative multiunit recordings (orange box in J) from the ventral thalamus of $Grn^{+/+}$, $Grn^{-/-}$, and $Grn^{-/-};C1qa^{-/-}$ mice. Black circle indicates stimulation artifact. Bottom: rate meters showing consistent evoked spike rate across sweeps of stimulations (x axis) relative to time (y axis).

(L) Peri-stimulus time histogram of the population data from six $Grn^{+/+}$, seven $Grn^{-/-}$, and four $Grn^{-/-};C1qa^{-/-}$ mice. Inset bottom: enlargement of the black dashed box in (L) showing the slope of the response is significantly different among genotypes (***p < 0.0001, F = 10.5554). Inset top: plot of the relative probability of eliciting AP firing frequencies among $Grn^{+/+}$, $Grn^{-/-}$ and $Grn^{-/-};C1qa^{-/-}$ mice analyzed by the Kolmogorov-Smirnov test ($Grn^{+/+}$ versus $Grn^{-/-}$, ***p < 0.0001, D = 0.5783; $Grn^{+/+}$ versus $Grn^{-/-};C1qa^{-/-}$, ***p < 0.0001, D = 0.4980; $Grn^{-/-}$ versus $Grn^{-/-};C1qa^{-/-}$, ***p < 0.0001, D = 0.7751). Error bars, SEM.

(M) Grooming activities in $Grn^{+/+}$, $Grn^{-/-}$, $C1qa^{-/-}$, and $Grn^{-/-};C1qa^{-/-}$ mice is expressed as percentage of total time. *p < 0.05, **p < 0.01; ns, not significant, Student's t test.

(N and O) Kaplan-Meier curve for skin lesion onset (N) and survival (O) in $Grn^{+/+}$, $Grn^{-/-}$, $C1qa^{-/-}$, and $Grn^{-/-};C1qa^{-/-}$ mice. *p < 0.05, ****p < 0.001; ns, not significant, Long-rank (Mantel-Cox) test.

See also Figures S4, S5 and S6, and Movie S1.

Figure 7. Microglial Pathology and CSF Complement Levels in FTLD *Grn* Mutation Carriers

(A–H) Immunostains of frontal cortex from control, FTLD *Grn* carriers and AD patients detect the presence of microglia and C1qa (A, B, D, E, G, and H). In addition, immunogold EM detects the presence of C1qa deposits at the synapses in FTLD *Grn* mutation carriers (C and F). Arrows in (A), (B), (D), (E), (G), and (H) indicate microglia. Arrowhead in (G) indicates an amyloid plaque and in (H) indicates a blood vessel (BV). Arrowheads in (C) and (F) indicate presynaptic terminals, and arrows in (F) indicate C1qa-positive immunogold particles in synapses.

(I) Quantification of Iba-1^{+} microglia in the frontal cortex of controls (n = 7), FTLD *Grn* carriers (n = 16), and AD patients (n = 8). ***p < 0.005, ****p < 0.001; ns, not significant, Student's t test.

(J) Quantification of CSF PGRN levels in controls and FTLD *GRN* carriers. Student's t test, ****p < 0.0001.

(K and L) ELISA assays for C1qa (K) and C3b (L) protein levels in the CSF of controls (n = 23) and FTLD *Grn* carriers (n = 19). Chi-square goodness-of-fit test to calculate R^2 and p values.

See also Figure S7 and Tables S2 and S3.

GRN mutations, and if so, whether complement activation could be a potential disease-specific biomarker. To this end, we examined microglial density in the frontal cortex of FTLD patients with *GRN* mutations (see the Supplemental Information and Table S2 for details). In addition, we included patients with sporadic Alzheimer's disease (AD) and age-matched control cases with no evidence of neurodegeneration (Table S2). In control frontal cortex, only few microglia with quiescent morphology were identified (Figure 7A). Most microglia in control individuals expressed very low levels of C1qa by immunohistochemistry, and no C1qa was identified near synapses by IEM (Figures 7B and 7C). In contrast, FTLD *GRN* carriers showed a marked increase in microglial density, most prominently affecting layers I–III of the frontal cortex (Figure 7D).

Similar to the microglia *Grn*−/− mouse brain, microglia in FTLD *GRN* carriers exhibited prominent reactive features and abundant C1qa deposits (Figure 7E). Furthermore, immunogold EM identified prominent C1qa signals near or at synapses in the frontal cortex of *GRN* mutation carriers (Figure 7F). To determine whether microglial infiltration in the frontal cortex of FTLD *GRN* carriers is disease-specific, we examined frontal cortex of AD patients and found that the majority of microglia in these cases appeared to surround the amyloid plaques, where abundant C1qa deposits were found (Figures 7G and 7H). On average, the microglial density in the frontal cortex of FTLD *GRN* carriers showed a 3- to 4-fold increase, whereas the microglial density in AD patients was similar to controls (Figure 7I).

The results from the frontal cortex of FTD *GRN* carriers raise the possibility that complement proteins might be released into the cerebrospinal fluid (CSF) and could serve as biomarkers to predict disease onset and/or progression. Indeed, the utility of CSF was underscored by the ∼70% drop in PGRN levels in FTLD patients with *GRN* mutations (Figure 7J). Interestingly, the levels of C1qa and C3b showed extensive overlapping in controls and FTLD *GRN* carriers, indicating that complement protein levels in CSF can be quite variable. However, as disease progressed in FTLD *GRN* carriers, the levels of C1qa and C3b progressively increased as cognitive functions declined (as determined by mini-mental status exam [MMSE] score) (Figures 7K and 7L). In contrast, analyses of previously published CSF data from AD patients (Smyth et al., 1994) showed that C1qa levels in AD patients were significantly lower than those in control and FTLD *GRN* carriers (controls: 479.5 ± 35.6, FTLD *GRN* carriers: 442.3 ± 33.0, AD: 268.0 ± 14.2, $p < 0.0001$, unpaired t test) (Figure S7A). Interestingly, as the MMSE declined in AD patients, the CSF C1qa levels showed progressive decrease (Figure S7B). Together, these results highlight the distinct differences in the microglia pathology and CSF complement protein levels between FTLD *GRN* carriers and AD patients.

DISCUSSION

PGRN Deficiency and Excessive Microglia Activation in the Aging Brain

Although PGRN has been implicated in lysosomal functions (Belcastro et al., 2011; Zhou et al., 2015), the exact mechanism remains poorly understood. Several lines of evidence from our study provide key mechanistic insights that PGRN regulates the formation and functions of lysosomes in the microglia. First, transcriptome profiling in $Grn^{+/+}$, $Grn^{+/-}$, and $Grn^{-/-}$ aging brains shows that loss of PGRN leads to progressive upregulation of genes that control lysosomal functions and the innate immunity response (Figures 1 and S1). Second, confocal microscopic analyses of cultured microglia show that abundant PGRN protein is expressed in the microglia and localized primarily in the Golgi apparatus, Sortilin$^+$ vesicles, and lysosomes, suggesting that PGRN might regulate intracellular trafficking and the formation of lysosomes. In support of this idea, $Grn^{-/-}$ microglia exhibit profound lysosomal defects that facilitate more efficient processing via the endolysosomal pathway. Such lysosomal phenotypes, working in conjunction with the upregulation of complement protein C3, promote proteolytic cleavage of C3 by C3 convertase in the lysosomes and lead to a marked increase in the release of biologically active C3 products, including C3b and iC3d (Figures 2, S2, and S3) (Liszewski et al., 2013; Naito et al., 2012). Finally, western blot analyses show age-dependent accumulation of C1qa and cleaved C3 products in the synaptosomes of $Grn^{-/-}$ brain. Consistent with these results, $Grn^{-/-}$ microglia show a marked increase in synaptic pruning activity in microglia-neuron co-cultures and in the ventral thalamus of $Grn^{-/-}$ brain (Figures 3, 4, 5, and 6). Together, these results support the idea that PGRN serves as an important "brake" to suppress excessive microglia activation in the aging brain by facilitating phagocytosis

and endolysosomal trafficking in microglia. Given the robust microglial activation in young mice exposed to the neurotoxin MPTP (Figure 2) (Martens et al., 2012), it is very likely that PGRN deficiency may have a broader role in suppressing microglia activation in other injury paradigms.

The identification of aberrant complement activation in $Grn^{-/-}$ microglia provides key mechanistic insights into the pathogenesis of neurodegeneration due to PGRN deficiency. The classical complement pathway serves as an important and well-recognized arm of the innate immunity surveillance system (Walport, 2001). Several previous studies indicate that complement-mediated synaptic pruning by microglia plays a critical role in the refinement of neural circuits during early postnatal development and in the normal aging process (Schafer et al., 2012; Shi et al., 2015; Stephan et al., 2013; Stevens et al., 2007). Although it has been postulated that excessive microglial activation may promote neurodegeneration (Aguzzi et al., 2013), the exact mechanisms remain unclear. Remarkably, our results show that loss of C1qa reduces synaptic pruning activity in $Grn^{-/-}$ microglia, reduces synapse loss, protects against hyperexcitability in the thalamocortical circuit, reduces behavioral abnormalities, and improves survival in $Grn^{-/-};C1qa^{-/-}$ mice. These results support that lysosomal dysfunctions and complement activation in $Grn^{-/-}$ microglia are the main drivers that directly promotes neurodegeneration in a mouse model of FTLD.

Circuit-Specific Synaptic Pruning by $Grn^{-/-}$ Microglia

One surprising neurodegenerative feature in $Grn^{-/-}$ brains is the selective loss of inhibitory synapses in the ventral thalamus, despite the fact that the accumulation of C1qa can be detected in both excitatory and inhibitory synapses (Figures 6 and S5). Such preferential elimination of inhibitory synapses by $Grn^{-/-}$ microglia is unprecedented in other neurodegenerative models. It is possible that differential expression of complement receptors or other recognition molecules in different synaptic subtypes may contribute to this selective phenotype. Alternatively, intrinsic properties of excitatory and inhibitory synapses may determine the efficacy of pruning by $Grn^{-/-}$ microglia. Regardless of the mechanism, the selective loss of inhibitory synapses in $Grn^{-/-}$ brain leads to increased excitability in the thalamocortical circuits.

Another remarkable finding in $Grn^{-/-}$ mice is the much more robust increase in microglia density in ventral thalamus, compared to other brain regions (Yin et al., 2010). This finding provides a neuroanatomical basis for the observed excessive grooming and OCD-like behaviors and is further supported by the well-established role of the ventral thalamus in integrating sensory inputs, frontostriatal circuits, and motor learning (Burguière et al., 2015). While it remains unclear why $Grn^{-/-}$ microglia show a preferential effect on the thalamocortical circuit, given the highly evolutionarily conserved function of this circuit in sensorimotor integration in mammals (Petersen, 2007), it is possible that similar pathology may contribute to the clinical manifestations in FTLD patients. Consistent with this idea, perseverative and compulsive behaviors are among the most important diagnostic criteria for FTLD (Rascovsky et al., 2011). Together, the results reveal previously unrecognized mechanisms of PGRN in microglia

function and how loss of PGRN may affect behaviors in a circuit-specific manner.

Despite the robust effects of deleting C1qa in mitigating several key neurodegenerative phenotypes in the aging $Grn^{-/-}$ mice, it is important to note that loss of C1qa does not completely rescue all the $Grn^{-/-}$ phenotypes. Although the microglial infiltration is significantly reduced in the ventral thalamus of $Grn^{-/-};C1qa^{-/-}$ mice, the microglial density is still significantly higher than age-matched $Grn^{+/+}$ mice (Figure 5). Many microglia in $Grn^{-/-};C1qa^{-/-}$ mice continue to exhibit morphological features similar to those seen in $Grn^{-/-}$ mice. Furthermore, despite the significant improvement in survival, $Grn^{-/-};C1qa^{-/-}$ mice still show a modest increase in mortality compared to control $Grn^{+/+}$ littermates. These results suggest that additional pathogenic factors, such as over-production of pro-inflammatory cytokines, other intrinsic microglia and/or neuronal defects, or intricate microglia-neuron interactions, may contribute to disease progression in $Grn^{-/-};C1qa^{-/-}$ mice in the absence of complement activation. For instance, the interacting network of upregulated genes in $Grn^{-/-}$ brain also identifies *Trem2* as a node that connects many other genes in the lysosomal and innate immunity pathways (Figure 1). Since the recent study indicates that TREM2 loss-of-function and TREM2-R47H variant attenuate lipid-sensing ability in microglia to mount a sustained response to neuronal injury in mouse AD models (Wang et al., 2015), these results raise the possibility that the elevated level of TREM2 in $Grn^{-/-}$ microglia may promote their synaptic pruning activity.

Microglia and Complement Activation as Critical Biomarkers for FTLD

One important neuropathologic feature in the frontal cortex of FTLD patients with *GRN* mutations is microglial activation, characterized by reactive morphology and excessive complement production (Figure 7). These findings are strikingly similar to those observed in $Grn^{-/-}$ mouse brain and raise the possibility that *GRN* mutations in FTLD patients may lead to chronic PGRN deficiency in brain tissues, resulting in a de facto PGRN loss-of-function phenotype similar to $Grn^{-/-}$ mice (Baker et al., 2006; Cruts et al., 2006). Another interesting finding is that CSF samples from FTLD patients with *Grn* mutations show progressive increases in C1qa and C3b that correlate with cognitive decline (Figure 7). In contrast, the histopathologic characteristics of C1qa distribution in the frontal cortex and the positive correlation of complement elevation in the CSF with the decline of MMSE in FTLD *GRN* carriers are distinctly different from those in AD patients. These results support the disease specificity of complement activation in FTLD (Figures 7 and S7) (Smyth et al., 1994) and further indicate that the underlying mechanisms that regulate the complement activation pathway in these two neurodegenerative diseases may be fundamentally different. These results underscore the importance of microglia and complement activation in human FTLD caused by *GRN* mutations and support the feasibility of developing strategies that target complement proteins as biomarkers to track disease progression and as valid therapeutic targets to mitigate neurodegeneration in FTLD.

EXPERIMENTAL PROCEDURES

Brain-Region-Specific Microarray and Bioinformatics Analyses

An aging cohort of $Grn^{+/+}$, $Grn^{+/-}$, and $Grn^{-/-}$ mice, ranging from 2, 6, 9, 12, and 18 months old, was used to characterize age-dependent changes in transcriptomes caused by PGRN deficiency. Mice were perfused with ice-cold PBS, and brains were removed and further dissected to isolate cerebral cortex, hippocampus, and cerebellum. Tissues were homogenized using the Bullet Blender (Next Advance) in Trizol (Invitrogen). RNA integrity was measured by running samples on a Bioanalyzer (Agilent). RNA samples were hybridized to Illumina Mouse8 version 2 microarray chips as previously described (Rosen et al., 2011). Network analyses were performed as previously described, and gene module merging was accomplished using the WGCNA package in R (Langfelder and Horvath, 2008). Differentially expressed genes within a given module were compared against the murine background for enrichment within gene ontology (GO) analysis (Table S1). These modules were further subjected to system-level functional analyses by determining their topographical overlap.

Human Brain Tissues and Cerebrospinal Fluid Samples

Frozen frontal lobe tissues were procured from controls with no known neurodegenerative diseases, FTLD patients with *GRN* mutations, and Alzheimer's disease (AD) patients. All cases were clinically and neuropathologically evaluated at the University of California San Francisco (UCSF), Northwestern University, and University of British Columbia. In addition, cerebrospinal fluid (CSF) samples were collected from controls and patients with *GRN* mutations and clinical diagnosis of FTD at UCSF and Italy. All human tissues and CSF samples were collected with informed consents and institutional review board (IRB) approvals. The demographic information, *GRN* mutations and pertinent clinical data of these cases are provided in Tables S2 and S3.

ACCESSION NUMBERS

The accession number for the microarray data reported in this paper is GEO: GSE75083.

SUPPLEMENTAL INFORMATION

Supplemental Information includes Supplemental Experimental Procedures, seven figures, three tables, and one movie and can be found with this article online at http://dx.doi.org/10.1016/j.cell.2016.04.001.

AUTHOR CONTRIBUTIONS

H.L., J.Z., H.-Y.H., M.K.C., and Y.S. designed and performed the experiments and analyzed data with E.J.H. J.T.P. and S.R.M. designed the electrophysiology experiments, S.R.M. performed recordings, and S.R.M. and J.T.P. analyzed data. L.M.H. and G.C. performed and analyzed microarray data. J.Z. and C.L.H. performed FACS sorting of microglia. F.G., G.C., K.W.K., S.A.S., M.C.O., and C.C.K. provided bioinformatics analyses. E.H.B., S.W., M.-M.M., R.R., I.R.M., W.W.S., A.K., B.L.M., B.B., R.G., R.V.F., and B.A.B. provided human samples and reagents. E.J.H. supervised the project, and H.L., J.Z., M.K.C., H.Y.H., Y.S., and E.J.H. wrote the manuscript.

REFERENCES

Aguzzi, A., Barres, B.A., and Bennett, M.L. (2013). Microglia: scapegoat, saboteur, or something else? Science *339*, 156–161.

Baker, M., Mackenzie, I.R., Pickering-Brown, S.M., Gass, J., Rademakers, R., Lindholm, C., Snowden, J., Adamson, J., Sadovnick, A.D., Rollinson, S., et al. (2006). Mutations in progranulin cause tau-negative frontotemporal dementia linked to chromosome 17. Nature *442*, 916–919.

Belcastro, V., Siciliano, V., Gregoretti, F., Mithbaokar, P., Dharmalingam, G., Berlingieri, S., Iorio, F., Oliva, G., Polishchuck, R., Brunetti-Pierri, N., and di Bernardo, D. (2011). Transcriptional gene network inference from a massive dataset elucidates transcriptome organization and gene function. Nucleic Acids Res. *39*, 8677–8688.

Burguière, E., Monteiro, P., Mallet, L., Feng, G., and Graybiel, A.M. (2015). Striatal circuits, habits, and implications for obsessive-compulsive disorder. Curr. Opin. Neurobiol. *30*, 59–65.

Carlin, R.K., Grab, D.J., Cohen, R.S., and Siekevitz, P. (1980). Isolation and characterization of postsynaptic densities from various brain regions: enrichment of different types of postsynaptic densities. J. Cell Biol. *86*, 831–845.

Castaneda, J.A., Lim, M.J., Cooper, J.D., and Pearce, D.A. (2008). Immune system irregularities in lysosomal storage disorders. Acta Neuropathol. *115*, 159–174.

Cotman, S.L., Karaa, A., Staropoli, J.F., and Sims, K.B. (2013). Neuronal ceroid lipofuscinosis: impact of recent genetic advances and expansion of the clinicopathologic spectrum. Curr. Neurol. Neurosci. Rep. *13*, 366.

Cruts, M., Gijselinck, I., van der Zee, J., Engelborghs, S., Wils, H., Pirici, D., Rademakers, R., Vandenberghe, R., Dermaut, B., Martin, J.J., et al. (2006). Null mutations in progranulin cause ubiquitin-positive frontotemporal dementia linked to chromosome 17q21. Nature *442*, 920–924.

Finch, N., Baker, M., Crook, R., Swanson, K., Kuntz, K., Surtees, R., Bisceglio, G., Rovelet-Lecrux, A., Boeve, B., Petersen, R.C., et al. (2009). Plasma progranulin levels predict progranulin mutation status in frontotemporal dementia patients and asymptomatic family members. Brain *132*, 583–591.

Fitzgerald, K.D., Welsh, R.C., Stern, E.R., Angstadt, M., Hanna, G.L., Abelson, J.L., and Taylor, S.F. (2011). Developmental alterations of frontal-striatal-thalamic connectivity in obsessive-compulsive disorder. J. Am. Acad. Child. Adolesc. Psychiatry *50*, 938–948.e3.

Ghidoni, R., Benussi, L., Glionna, M., Franzoni, M., and Binetti, G. (2008). Low plasma progranulin levels predict progranulin mutations in frontotemporal lobar degeneration. Neurology *71*, 1235–1239.

Götzl, J.K., Mori, K., Damme, M., Fellerer, K., Tahirovic, S., Kleinberger, G., Janssens, J., van der Zee, J., Lang, C.M., Kremmer, E., et al. (2014). Common pathobiochemical hallmarks of progranulin-associated frontotemporal lobar degeneration and neuronal ceroid lipofuscinosis. Acta Neuropathol. *127*, 845–860.

Kao, A.W., Eisenhut, R.J., Martens, L.H., Nakamura, A., Huang, A., Bagley, J.A., Zhou, P., de Luis, A., Neukomm, L.J., Cabello, J., et al. (2011). A neurodegenerative disease mutation that accelerates the clearance of apoptotic cells. Proc. Natl. Acad. Sci. USA *108*, 4441–4446.

Langfelder, P., and Horvath, S. (2008). WGCNA: an R package for weighted correlation network analysis. BMC Bioinformatics *9*, 559.

Liszewski, M.K., Kolev, M., Le Friec, G., Leung, M., Bertram, P.G., Fara, A.F., Subias, M., Pickering, M.C., Drouet, C., Meri, S., et al. (2013). Intracellular complement activation sustains T cell homeostasis and mediates effector differentiation. Immunity *39*, 1143–1157.

Martens, L.H., Zhang, J., Barmada, S.J., Zhou, P., Kamiya, S., Sun, B., Min, S.W., Gan, L., Finkbeiner, S., Huang, E.J., and Farese, R.V., Jr. (2012). Progranulin deficiency promotes neuroinflammation and neuron loss following toxin-induced injury. J. Clin. Invest. *122*, 3955–3959.

Naito, A.T., Sumida, T., Nomura, S., Liu, M.L., Higo, T., Nakagawa, A., Okada, K., Sakai, T., Hashimoto, A., Hara, Y., et al. (2012). Complement C1q activates canonical Wnt signaling and promotes aging-related phenotypes. Cell *149*, 1298–1313.

Paolicelli, R.C., Bolasco, G., Pagani, F., Maggi, L., Scianni, M., Panzanelli, P., Giustetto, M., Ferreira, T.A., Guiducci, E., Dumas, L., et al. (2011). Synaptic pruning by microglia is necessary for normal brain development. Science *333*, 1456–1458.

Parkhurst, C.N., Yang, G., Ninan, I., Savas, J.N., Yates, J.R., 3rd, Lafaille, J.J., Hempstead, B.L., Littman, D.R., and Gan, W.B. (2013). Microglia promote learning-dependent synapse formation through brain-derived neurotrophic factor. Cell *155*, 1596–1609.

Paz, J.T., Bryant, A.S., Peng, K., Fenno, L., Yizhar, O., Frankel, W.N., Deisseroth, K., and Huguenard, J.R. (2011). A new mode of corticothalamic transmission revealed in the Gria4(-/-) model of absence epilepsy. Nat. Neurosci. *14*, 1167–1173.

Paz, J.T., Davidson, T.J., Frechette, E.S., Delord, B., Parada, I., Peng, K., Deisseroth, K., and Huguenard, J.R. (2013). Closed-loop optogenetic control of thalamus as a tool for interrupting seizures after cortical injury. Nat. Neurosci. *16*, 64–70.

Petersen, C.C. (2007). The functional organization of the barrel cortex. Neuron *56*, 339–355.

Ransohoff, R.M., and Perry, V.H. (2009). Microglial physiology: unique stimuli, specialized responses. Annu. Rev. Immunol. *27*, 119–145.

Rascovsky, K., Hodges, J.R., Knopman, D., Mendez, M.F., Kramer, J.H., Neuhaus, J., van Swieten, J.C., Seelaar, H., Dopper, E.G., Onyike, C.U., et al. (2011). Sensitivity of revised diagnostic criteria for the behavioural variant of frontotemporal dementia. Brain *134*, 2456–2477.

Ratnavalli, E., Brayne, C., Dawson, K., and Hodges, J.R. (2002). The prevalence of frontotemporal dementia. Neurology *58*, 1615–1621.

Rosen, E.Y., Wexler, E.M., Versano, R., Coppola, G., Gao, F., Winden, K.D., Oldham, M.C., Martens, L.H., Zhou, P., Farese, R.V., Jr., and Geschwind, D.H. (2011). Functional genomic analyses identify pathways dysregulated by progranulin deficiency, implicating Wnt signaling. Neuron *71*, 1030–1042.

Schafer, D.P., Lehrman, E.K., Kautzman, A.G., Koyama, R., Mardinly, A.R., Yamasaki, R., Ransohoff, R.M., Greenberg, M.E., Barres, B.A., and Stevens, B. (2012). Microglia sculpt postnatal neural circuits in an activity and complement-dependent manner. Neuron *74*, 691–705.

Shi, Q., Colodner, K.J., Matousek, S.B., Merry, K., Hong, S., Kenison, J.E., Frost, J.L., Le, K.X., Li, S., Dodart, J.C., et al. (2015). Complement C3-deficient mice fail to display age-related hippocampal decline. J. Neurosci. *35*, 13029–13042.

Sleegers, K., Brouwers, N., Van Damme, P., Engelborghs, S., Gijselinck, I., van der Zee, J., Peeters, K., Mattheijssens, M., Cruts, M., Vandenberghe, R., et al. (2009). Serum biomarker for progranulin-associated frontotemporal lobar degeneration. Ann. Neurol. *65*, 603–609.

Smith, K.R., Damiano, J., Franceschetti, S., Carpenter, S., Canafoglia, L., Morbin, M., Rossi, G., Pareyson, D., Mole, S.E., Staropoli, J.F., et al. (2012). Strikingly different clinicopathological phenotypes determined by progranulin-mutation dosage. Am. J. Hum. Genet. *90*, 1102–1107.

Smyth, M.D., Cribbs, D.H., Tenner, A.J., Shankle, W.R., Dick, M., Kesslak, J.P., and Cotman, C.W. (1994). Decreased levels of C1q in cerebrospinal fluid of living Alzheimer patients correlate with disease state. Neurobiol. Aging *15*, 609–614.

Stephan, A.H., Madison, D.V., Mateos, J.M., Fraser, D.A., Lovelett, E.A., Coutellier, L., Kim, L., Tsai, H.H., Huang, E.J., Rowitch, D.H., et al. (2013). A dramatic increase of C1q protein in the CNS during normal aging. J. Neurosci. *33*, 13460–13474.

Stevens, B., Allen, N.J., Vazquez, L.E., Howell, G.R., Christopherson, K.S., Nouri, N., Micheva, K.D., Mehalow, A.K., Huberman, A.D., Stafford, B., et al. (2007). The classical complement cascade mediates CNS synapse elimination. Cell *131*, 1164–1178.

Vázquez, C.L., and Colombo, M.I. (2009). Assays to assess autophagy induction and fusion of autophagic vacuoles with a degradative compartment, using monodansylcadaverine (MDC) and DQ-BSA. Methods Enzymol. *452*, 85–95.

Walport, M.J. (2001). Complement. First of two parts. N. Engl. J. Med. *344*, 1058–1066.

Wang, Y., Cella, M., Mallinson, K., Ulrich, J.D., Young, K.L., Robinette, M.L., Gilfillan, S., Krishnan, G.M., Sudhakar, S., Zinselmeyer, B.H., et al. (2015). TREM2 lipid sensing sustains the microglial response in an Alzheimer's disease model. Cell *160*, 1061–1071.

Yin, F., Banerjee, R., Thomas, B., Zhou, P., Qian, L., Jia, T., Ma, X., Ma, Y., Iadecola, C., Beal, M.F., et al. (2010). Exaggerated inflammation, impaired host defense, and neuropathology in progranulin-deficient mice. J. Exp. Med. *207*, 117–128.

Yoshimori, T., Yamamoto, A., Moriyama, Y., Futai, M., and Tashiro, Y. (1991). Bafilomycin A1, a specific inhibitor of vacuolar-type H(+)-ATPase, inhibits acidification and protein degradation in lysosomes of cultured cells. J. Biol. Chem. *266*, 17707–17712.

Zhang, B., and Horvath, S. (2005). A general framework for weighted gene coexpression network analysis. Stat. Appl. Genet. Mol. Biol. *4*, Article17.

Zhang, Y., Chen, K., Sloan, S.A., Bennett, M.L., Scholze, A.R., O'Keeffe, S., Phatnani, H.P., Guarnieri, P., Caneda, C., Ruderisch, N., et al. (2014). An RNA-sequencing transcriptome and splicing database of glia, neurons, and vascular cells of the cerebral cortex. J. Neurosci. *34*, 11929–11947.

Zhou, X., Sun, L., Bastos de Oliveira, F., Qi, X., Brown, W.J., Smolka, M.B., Sun, Y., and Hu, F. (2015). Prosaposin facilitates sortilin-independent lysosomal trafficking of progranulin. J. Cell Biol. *210*, 991–1002.